

Unveiling the Relationship Between Structure and Dynamics in Complex Networks

Cesar H. Comin, João B. Bunoro, Matheus P. Viana and Luciano da F. Costa¹

¹*Institute of Physics at São Carlos,
University of São Paulo, São Carlos,
São Paulo, 13560-970 Brazil*

(Dated: November 13, 2021)

Over the last years, a great deal of attention has been focused on complex networked systems, characterized by intricate structure and dynamics [1–6]. The latter has been often represented in terms of overall statistics (e.g. average and standard deviations) of the time signals [1]. While such approaches have led to many insights, they have failed to take into account that signals at different parts of the system can undergo distinct evolutions, which cannot be properly represented in terms of average values. A novel framework for identifying the principal aspects of the dynamics and how it is influenced by the network structure is proposed in this work. The potential of this approach is illustrated with respect to three important models (Integrate-and-Fire, SIS and Kuramoto), allowing the identification of highly structured dynamics, in the sense that different groups of nodes not only presented specific dynamics but also felt the structure of the network in different ways.

Given that complex systems are almost invariantly composed by a large number of interacting elements, they can be effectively represented and modeled in terms of complex networks [7, 8]. With this mapping, their structural and dynamical properties can be extracted and investigated. Typically, the structure of such networks is quantified in terms of several measurements [9], reflecting different properties of the respective topology (e.g. node degree, shortest paths, centralities) and geometry (e.g. arc length distances, angles, spatial density).

A great deal of the investigations about structure and function in complex systems has focused on trying to predict the dynamics from specific structural features [1, 10, 11]. Such an ability would provides the means for effectively controlling real-world systems. Despite the growing number of works devoted to this problem, the knowledge about the relationship between the structural and dynamical properties remains incipient because of two main reasons: (a) dynamics is often summarized in terms of global statistics, overlooking the intricacies of dynamics; and (b) the investigation often focuses on linear relationships such as correlations between structural and dynamical features.

The present work is aimed at addressing these limitations through a comprehensive and systematic procedure, involving three steps described as following. First, we use the multivariate statistical approach known as Principal Component Analysis (PCA) [12] in order to identify the most important features of the dynamics unfolding at every network node. Then, we apply a procedure for checking at what an extent they are determined by *any* structural property of the system. Therefore, we first identify the dynamical features that are affected by the network structure and thereafter probe the effect of a given set of structural measurements on those features (see supplementary Figure 1). We found that the time signals are organized into well-defined patterns (see box for a simple example of structured dynamics), which is henceforth called *structured dynamics*.

After the time signal $x_i(t)$ at each node i is recorded along T consecutive discrete time instants ($t = 1, 2, \dots, T$), the PCA methodology can be applied in order to obtain linear combinations of the signal components (new random variables) that can be understood as new measurements $PCA_i^{(1)}, PCA_i^{(2)}, \dots, PCA_i^{(M)}$ ($M \leq T$) characterizing each individual signal i . These measurements are completely uncorrelated and correspond to respective projections of the original space along axes that are optimally aligned along the directions of maximum variation of the dynamics. Therefore, the PCA provides a compact and effective description of the original time signals. In case they are correlated, just a few principal axes are required for explaining the most relevant aspects of the original dynamics. The present work focuses attention on this category of dynamical systems.

Having identified the most relevant aspects of the time signals, it is now important to check at what an extent each of the dynamical variables $PCA^{(m)}$ is being influenced by *any* of the structural aspects of the system under study. Thus, the method relies on no specific structural measurements whatsoever. First we assume that the time signal of a node i can be expressed as in Equation .

$$x_i(t+1) = F(\{x_j(t)\}),$$

where j indexes the neighbors of i , and the initial condition is $x_i(0) = \xi_i$. Note that the system is Markovian, time invariant and that the dynamic function F is assumed to be identical at each of the network nodes. Therefore, the dynamics at a node i depends on three elements: (i) the function F , (ii) the initial condition $\vec{\xi}$, and (iii) the topology of the network, given by the adjacency matrix \mathbf{A} . The null hypothesis is that the time signals cannot be discriminated

one another. The given network is subjected to a large number of simulations starting with different initial conditions $\vec{\xi}$. Then, the density functions $P(PCA^{(m)})$ for each principal dynamical feature $PCA^{(m)}$ are estimated and used as references. Thus, each of these density functions provides an estimate of the values obtained for the feature $PCA^{(m)}$ considering all the network nodes. Also, the individual density functions $P_i(PCA_i^{(m)})$ of the values of $PCA_i^{(m)}$ are estimated considering each node i individually. In order to test whether the structural features produce distinct dynamical behavior at node level, we introduce the index, $\alpha_i^{(m)}$, between $P(PCA^{(m)})$ and $P_i(PCA_i^{(m)})$, which is defined as the Euclidean distance between the respective densities. In other words, the value of α_i expresses how much the node i deviates from the null hypothesis. In case $\alpha_i^{(m)}$ is significantly small, the dynamical property $PCA_i^{(m)}$ at node i is understood not to be discriminated by any structural features, confirming the null hypothesis.

For each dynamical feature $PCA^{(m)}$ for which the null hypothesis is not verified, we then quantify how much it is related to each of a predefined set of structural measurements $s^{(1)}, s^{(2)}, \dots, s^{(S)}$. To do so, we calculate the dispersion of α along the measurement, weighted by its density. This is conveniently given by the conditional entropy (or equivocation [14]) between s and α .

In order to illustrate the proposed approach, we resort to three well-known types of dynamics in complex systems, namely integrate-and-fire [15, 16], epidemics spreading (SIS) [17, 18], and synchronization (Kuramoto oscillators) [19–21] (see the Box). Although the proposed methodology can be applied to any regime, we consider the steady-state values of the signals in the Erdős-Rényi (ER) model.

We start by investigating the *integrate-and-fire* dynamics in which each node is understood as a neuron undergoing the McCulloch and Pitts integrate-and-fire dynamics [22, 23]. The binary time signal (firing spikes) of each node is recorded and represented as a vector. PCA is then applied over this ensemble of vectors to project the data onto the eigenvectors associated with the three largest eigenvalues. Figure 8(a) shows the PCA projections of the time signals, with the colors corresponding to the node degrees (see also the supplementary Figure 2). Remarkably, the nodes resulted organized according to a well-defined geometrical pattern. Also shown in Figure 8 are the densities (Figs. 8b,d) and average entropies (Figs. 8c,e) of the original signals after being further projected into two dimensions. Note that the 2D PCA projections include groups of nodes organized as ‘cords’ (see supplementary Figure 3). The obtained 3D projection can be divided into three main regions: (i) a relatively sparse conic ‘head’; (ii) a densely populated ‘waist’; and (iii) a relatively dense and complex ‘tail’. We observe that the density peaks occur at low entropy places. This suggests that the system dynamics tends to unfold so as to favor more ordered (i.e. lower entropy) time signals.

Another dynamical process considered in this paper is the *Susceptible-Infected-Susceptible* (SIS) model [24] that is used to investigate epidemics spreading on networked systems. For this dynamical process, the time series associated to each node is also binary. Figure 8(f) shows the PCA projection of the SIS dynamics (node degrees mapped into colors), as well as the respective further two-dimensional projections into the $PCA(1) \times PCA(2)$ plane. The resulting PCA pattern is much simpler than that obtained for the integrate-and-fire dynamics, now containing just an eye-shaped volume. A cord can also be identified in this projection (see supplementary Figure 3). A similar trend is observed between the time signal density and entropy (Figure 8g,h).

The third dynamics investigated in this work is the *Kuramoto dynamics* [20], whose PCA projection is shown in Figure 8(i), with the respective one-dimensional projection given in (j). It is clear from these results that the Kuramoto dynamics yielded the simplest PCA projection, in the sense that most of the signals variance is explained by $PCA(1)$. We also found that the Kuramoto dynamics tends to yield cords which are related to the natural frequencies of the nodes, parametrized by the respective relative phases (see supplementary Figure 4).

In the second step of our methodology, we evaluated the $\alpha_i^{(m)}$ for each of the new measurements $PCA^{(m)}$, as illustrated in Figures 9. The statistical significance of the α values was obtained by using a random null model (see supplementary Figure 5). First, several simulations were performed for varying random initial conditions $\vec{\xi}$, from which the reference histograms $P(PCA^{(1)})$, $P(PCA^{(2)})$ and $P(PCA^{(3)})$ in Figure 9(a-c) were obtained for the integrate-and-fire dynamics. These densities were also estimated for each node separately. For instance, in Figure 9(d-f), (g-i), and (j-l), we illustrate the densities of $PCA^{(1)}$, $PCA^{(2)}$ and $PCA^{(3)}$, respectively, for three randomly chosen nodes. The small values of α obtained in (g) indicate that this nodes is not being indistinctly influenced by any structural features of the network. On the other hand, larger values of α , such as those in (f,i,k,l) corroborate that the time signals at those respective nodes are greatly affected by the network structure. The overall α densities are shown in Figure 9(m-o) for integrate-and-fire, (p,q) for SIS, and (r) for Kuramoto. Remarkably, the wide dispersion of α values obtained for most cases confirms that the structural influence on the dynamics can vary strongly from one node to another. It is also clear from these results that the $PCA^{(3)}$ of the integrate-and-fire dynamics, as well as the $PCA^{(2)}$ of the SIS dynamics are the dynamical features mostly affected by the topology of the network. As expected, because of the adopted strong coupling, the Kuramoto dynamics resulted to be largely independent of the network structure, which was duly identified by the proposed methodology. This is confirmed by the rather small values of α shown in the density in Figure 9(r). A stronger influence of the topology was verified for a weaker coupling (see

supplementary Figure 6).

We now proceed to the third step, obtaining scatterplots of the $\alpha^{(m)}$ versus some topological measurements. The respective conditional entropies are then estimated in order to quantify the degree at which the α values are being explained by each of the measurements. The scatterplots respectively to the smallest conditional entropies (see Table I) are depicted in Figure 10. In case of the integrate-and-fire dynamics (Fig. 10a-c), we have that the eigenvector centrality was the topological feature that most strongly affected all the three principal component variables. As can be seen in the scatterplot for $\alpha^{(3)}$ versus EC (Fig. 10c), the influence of the topology on the $PCA^{(3)}$ measurement is felt more strongly for the nodes with lower EC values. As shown in Figure 10(d,e), respective to the SIS dynamics, the degree was the measurement most directly related to the two principal variables. Other measurements also were found to be related to the 2D PCA projections (see supplementary Figure 7). Remarkably, the values of $\alpha^{(1)}$ and $\alpha^{(2)}$ present a low peak at values of degree similar to the average network degree ($\langle k \rangle = 10$), meaning that both $PCA^{(1)}$ and $PCA^{(2)}$ variables of the SIS tend to feel the topology only for nodes with degree distinct from $\langle k \rangle$. Although the Kuramoto dynamics resulted unaffected by the network structure, the accessibility was the topological feature that yielded the smallest conditional entropy.

All in all, we have proposed a new methodology for investigating the relationship between structure and dynamics in complex networked systems. The reported approach relies on two critical concepts, namely the consideration of the structure/dynamics relationship at the individual node level and also along different values of specific structural measurements. These concepts allowed the separation of the intermixing effects that would be otherwise obtained by using traditional approaches where both structure and dynamics are summarized in terms of global statistics. The obtained results corroborated the validity and importance of these hypotheses. Moreover, despite the uniformity of the ER topology, we identified a highly structured dynamics. In the case of the integrate-and-fire and the SIS dynamics, we found that the PCA regions with higher density of nodes tended to present low signal entropy, which suggests that the dynamics is related to signal uniformity.

I. SUPPLEMENTARY MATERIAL

A. Diagram

The framework proposed in the present article for investigating the relationship between structure and dynamics in complex systems is summarized by the flow diagram in Figure 1. First, during the simulation stage, the original network is subjected to a total of N_C random initial conditions and the time signals for each node is recorded after the steady state has been reached. The next step involves the extraction of PCA dynamics features from the time signals. These features are then used to obtain the respective reference histogram. The Euclidean distances between this reference histogram and the node histograms are obtained and used to estimate the α values for each node with respect to each dynamical feature. Measurements T_i of the structure of the network are also estimated and used to obtain the scatterplots $\alpha \times T_i$.

It should be observed that the orientation of the PCA axes is undetermined, because the negative of an eigenvector is also an eigenvector associated to the same eigenvalue. Therefore, in order to provide a stable reference, we obtained a set of eigenvectors for the large network (10000 nodes) and adopted then for all subsequent projections.

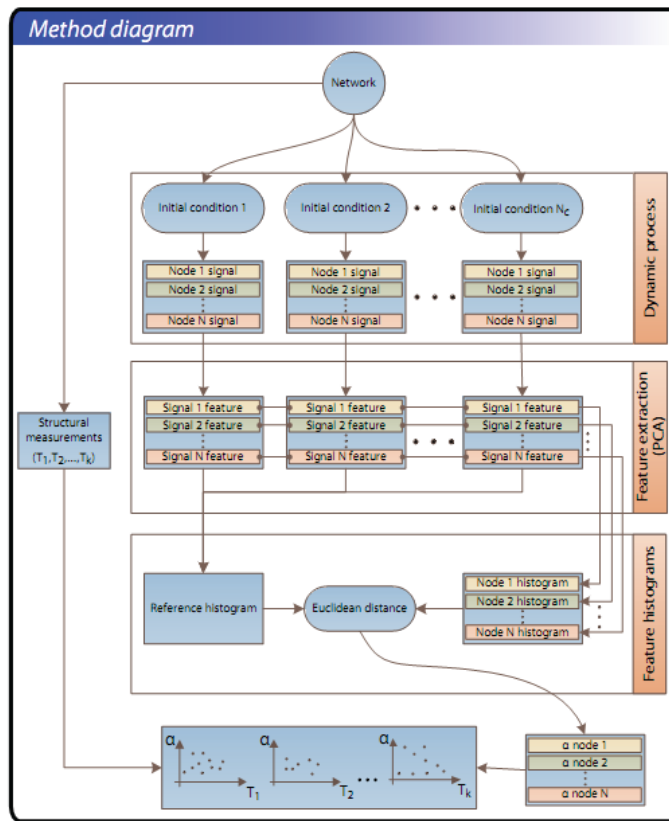


FIG. 1: Flow diagram of the framework proposed in this article for investigating the relationship between structure and dynamics of complex systems.

B. Integrate-and-Fire time signals

The integrate-and-fire dynamics has been extensively investigated in complex systems because not only of its biological inspiration (i.e. as a simplified model of neuronal networks), but also as a consequence of its rich behavior [1–6]. Though initial investigations focused on more regular topologies such as layered systems and lattices [7, 8], much attention has been driven to the study of integrate-and-fire unfolding in complex networks [22, 23]. Given that different network models are characterized by specific topological features, a fundamental question arises regarding the relationship between such structural properties and the respective dynamics. Remarkable related results have been obtained through the application of the methodology proposed in this article. Figure 2 shows the three-dimensional PCA representation of the integrate-and-fire dynamics unfolding in an ER network with 10000 nodes and average degree 10. The integrate-and-fire realization considered initial conditions drawn uniformly within the range $[0, \tau + 1]$, with $\tau = 8$. The time signals were recorded along 1000 steps after the system had reached steady state.

The nodes were colored according to their degree, which resulted stratified along the $PCA^{(3)}$ axis. Examples of respective time signals are shown on the righthand side of Figure 2. Interestingly, the time signals tended to be distributed along the $PCA^{(3)}$ axis in terms of their respective average frequency. The top of the PCA structure is populated by signals with maximum frequency, i.e. a firing spike at each time instant. The frequency decreases as one moves downwards along the $PCA^{(3)}$ axis, such that the lowest frequency signals are found at the bottom (tail) of the PCA structure. The largest number of time signals (about 40%) were found to have average period of 2 cycles and to be distributed along the ‘waist’ of the PCA structure. As it becomes clear from Figure 3c, the time signals tended to be organized in groups with similar frequencies corresponding to integer number of cycles, in a way that reminds harmonic frequency distribution in a linear system. This finding implies that systems undergoing integrate-and-fire dynamics with similar parameters will have most neurons firing at 2 cycles, with the others tending to have multiple integer periods of oscillations. This interesting finding is related to the fact that the investigated dynamics in the ER structure tends to favor the uniformity of the time signals, as reflected in the respective entropy. Particularly remarkable is that such structured dynamics, including marked clusters of time signals, arose despite the structural

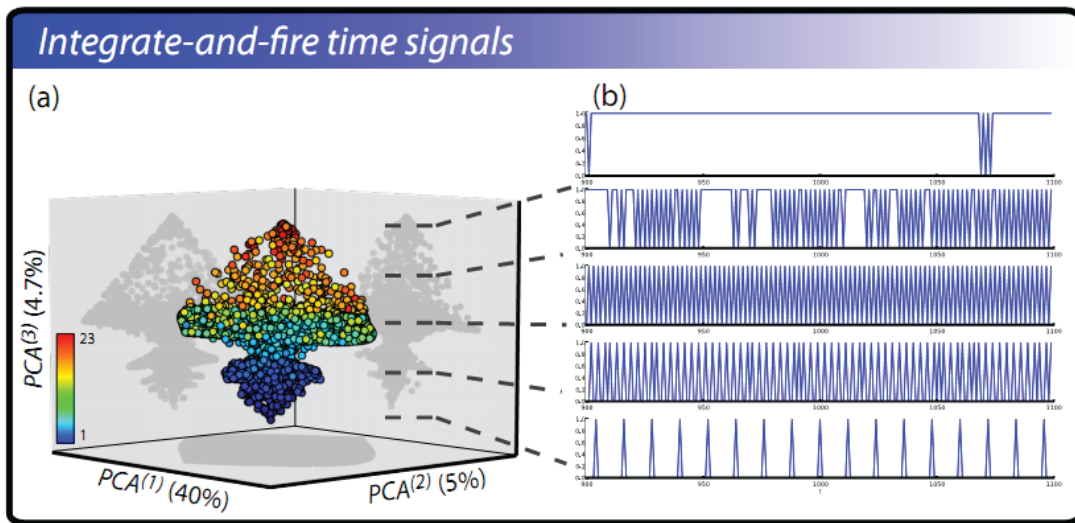


FIG. 2: (a) The 3d PCA projections of the integrate-and-fire dynamics unfolding in an ER network. (b) Examples of time signals obtained for the stratifications of the dynamics along the $PCA^{(3)}$ axis. Observe that the frequency of the signals tends to decrease with lower values of $PCA^{(3)}$.

uniformity of the ER network.

C. Cords

In order to explain the organization of signals along the cords in the PCA projections, we develop now a simple formulation for the values of $PCA^{(1)}$ and $PCA^{(2)}$, which we will call x and y for simplicity. First, let us assume we have the signal showed in Figure 3(a), which can be expressed as

$$s(t) = \sum_{i=1}^N \delta_{t,v_i}, \quad (1)$$

where, N is the total number of spikes in the considered time interval, the i -th element of the \vec{v} identifies the instant of the i -th spike. We can write the following rule for the elements of \vec{v}

$$v_i = \begin{cases} 2i - 1 & \text{if } 1 \leq i < h \\ 2i & \text{if } h \leq i \leq N. \end{cases} \quad (2)$$

On the other hand, the first and second eigenvectors of the *integrate-and-fire* and SIS dynamics can be expressed as

$$e_1(t) = (-1)^t \quad (3)$$

and

$$e_2(t) = (-1)^t \cos\left(\frac{t\pi}{T}\right), \quad (4)$$

where $1 \leq t \leq T$, and T is the size of the time window. Therefore, we can estimate the values of x and y considering the inner-product of the signal and the respective eigenvector:

$$x = \sum_{t=1}^T (-1)^t s(t) \quad (5)$$

and

$$y = \sum_{t=1}^T (-1)^t \cos\left(\frac{t\pi}{T}\right) s(t). \quad (6)$$

Substituting Equation 1, we find the PCA projections as a function of the hole position, h

$$x(h) = N - 2(h + 1) \quad (7)$$

and

$$y(h) = \sum_{i=h}^N \cos\left(\frac{2i\pi}{T}\right) - \sum_{i=1}^{h-1} \cos\left(\frac{(2i-1)\pi}{T}\right). \quad (8)$$

In Figure 3(b) and 3(c) we show the plot of y in terms of x (blue curves) for different values of h considering the integrate-and-fire and SIS dynamics, respectively. It is interesting to observe that if we consider the first element of the time signal as being zero (instead of one), the resulting curves corresponds to the red curves.

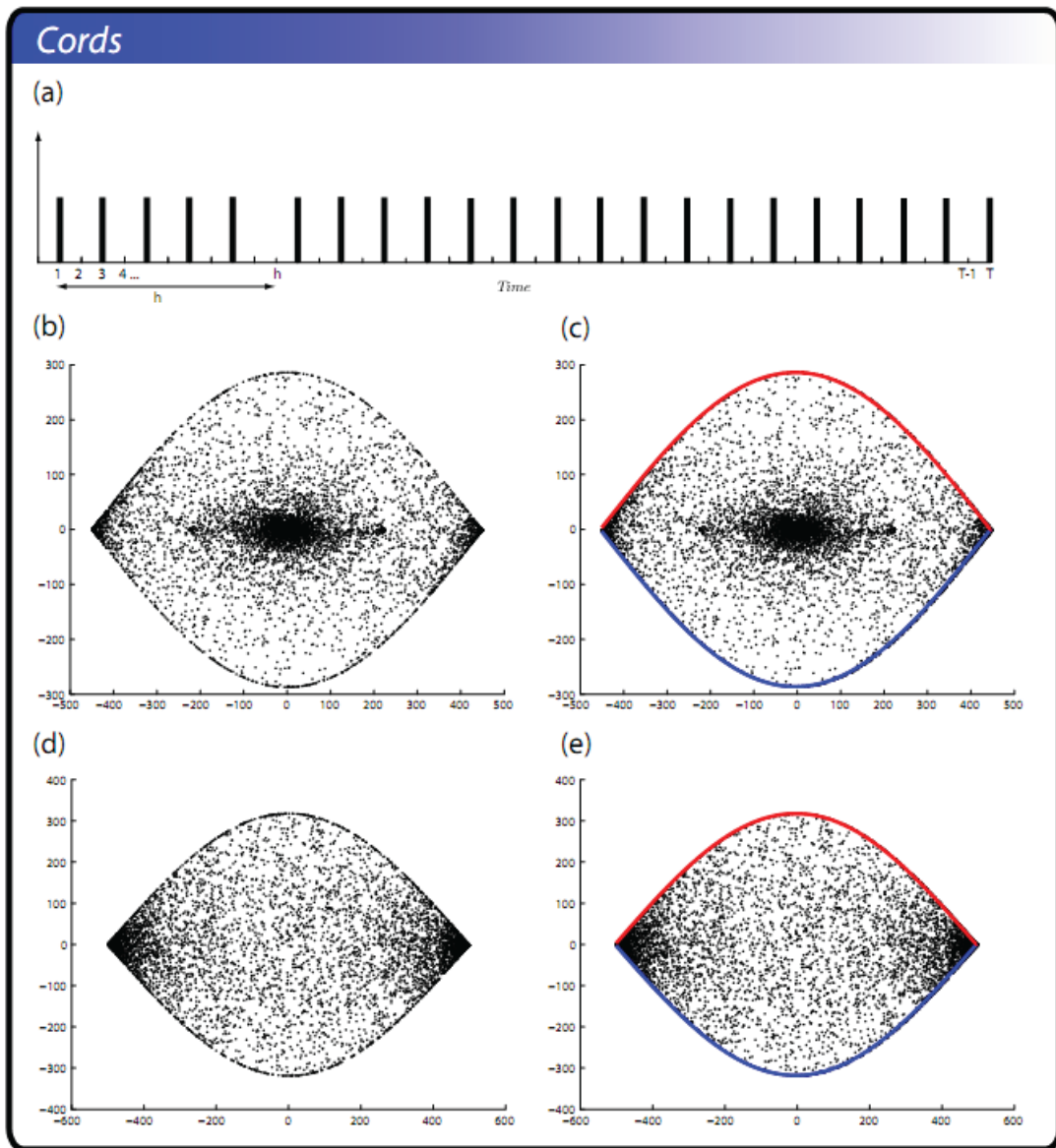


FIG. 3: (a) General form of the one-hole (two consecutive zeros) time signal. The 2D PCA projection of the (b) integrate-and-fire dynamics and (d) SIS. The same, (c) and (e) respectively, with the analytical parametric curves approximating the cords

D. Phases in Kuramoto

A different parametric configuration of the Kuramoto dynamics was used in order to further illustrate the potential of the PCA methodology in identifying meaningful properties of the dynamics. Three groups of nodes in an ER network with 1000 nodes were assigned specific natural frequencies, with weak coupling ($\lambda = 0.5$). Figure 4(a) depicts the 2D PCA projections obtained for the respective dynamics. The colors in this figure identify each of the frequency groups. Their respective projections are also shown in Figures 4 (b-d). The colors in these three figures identify the relative phase of the time signals at each node. Figure 4(e) illustrates five characteristic time signals obtained along the cord in Figure 4(d).

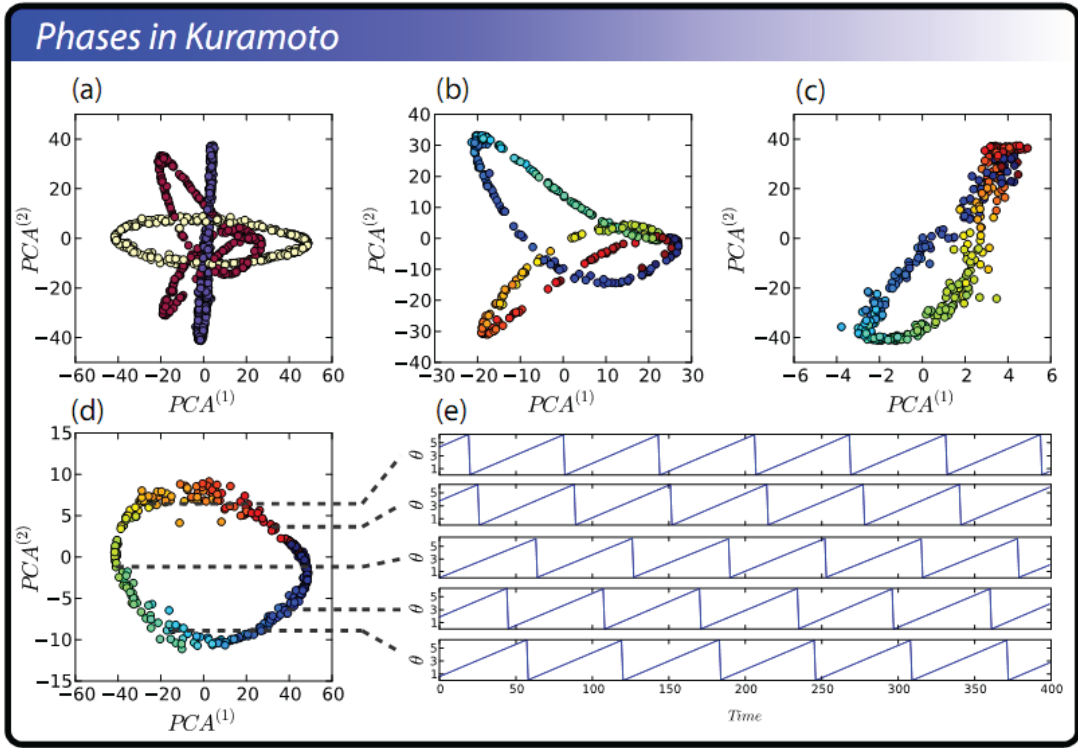


FIG. 4: Illustration of the distribution of phases of the time signals along the cords yielded by the Kuramoto dynamics for an ER network with three frequency groups.

E. Statistical Significance of α

In order to obtain a level of statistical significance for the values of α produced by our simulations, we also consider the distribution of α values that would be obtained in the case of a random null model. In this model the value of α for each node was obtained by sampling, through Monte Carlo, N_C PCA features from the reference histogram. Figure 5 illustrates this approach with respect to the $PCA^{(2)}$ variable in integrate-and-fire dynamics. The histogram for the null model, shown in red, is well-fitted by a log-normal distribution. The histogram of α values obtained for the integrate-and-fire configuration is shown in gray. By comparing the latter histogram with the fitted log-normal distribution, it is possible to calculate the significance level assuming 0.001 confidence. In this specific case, we obtained $\alpha^* = 0.053$, which corresponds to the probability of obtaining a value of α larger than α^* by chance.

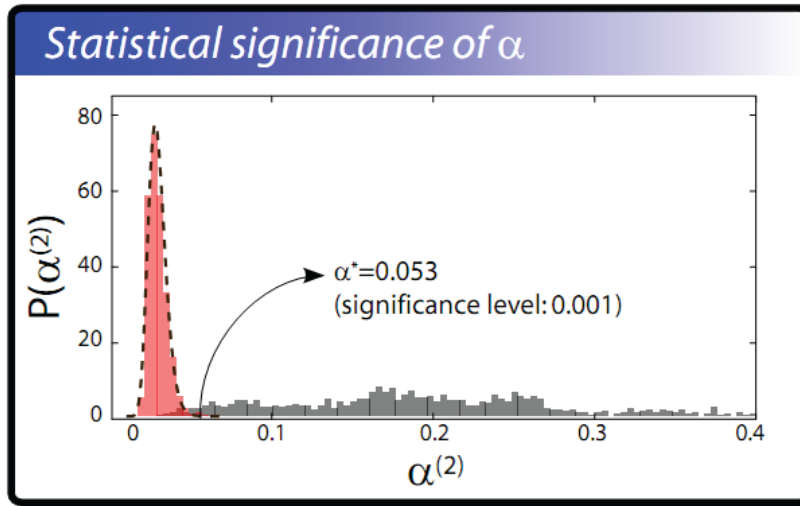


FIG. 5: Illustration of the construction used to obtain levels of statistical significance for the values of α .

F. Effect of coupling in the Kuramoto dynamics

To illustrate the proposed methodology, we considered in the main article a strongly coupled version of the Kuramoto oscillator. Here we provide complementary results with respect to a less intensely coupled configuration. Figures 6 (a) and (c) show the histograms of α obtained for this type of dynamics considering relatively weak ($\lambda = 1.75$) and strong ($\lambda = 4.00$) couplings. The histograms of α obtained for the null reference model are shown in Figures 6 (b) and (d), respectively. It is clear from these results that the values of α are substantially higher than those obtained for the null model in the case of the less strongly coupled Kuramoto simulations, while being undistinguishable in the more strongly coupled case. This means that in the less strongly coupled Kuramoto configuration the dynamics at each node is differentiated by the network structure, which is not observed in the other configuration.

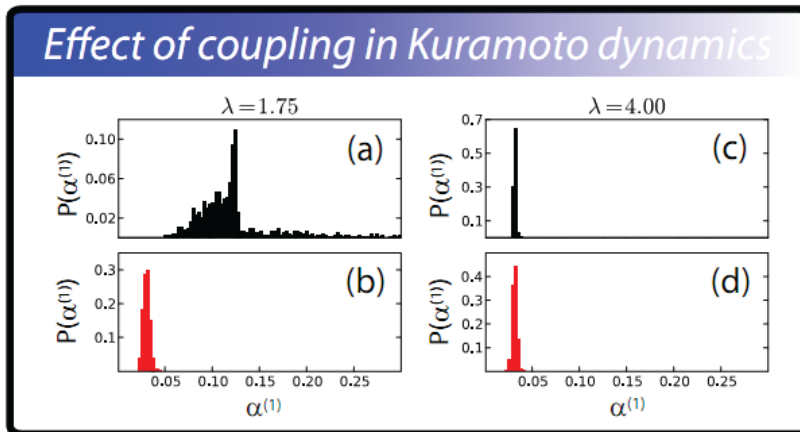


FIG. 6: Effect of the coupling in the Kuramoto dynamics. As expected, a strong coupling makes the dynamics at each node not to be differentiated by any structural features of the network.

G. Topological measurements over the 2D PCA projection of the SIS dynamics

So as to better understand the structure versus dynamics relationship in the SIS model, we mapped the values of the six considered specific topological features onto the 2D PCA projections obtained for this model, as shown in Figure 7. In each case, the projected points were separated into two main subsets: one corresponding to the border of the eye-shaped pattern (a ‘chord’) and the other to the remainder region. The histograms of the measurements for these two groups are also shown in Figure 7 respectively to each 2D projection. It is clear from these results that the time signals in these two groups tend to be well-separated with respect to their degree, eigenvalue centrality, and accessibility. More specifically, nodes with high values of these three measurements tend to be found along the chord. Given that low accessibility values have been found to be associated to the border of complex networks [25], it is possible that the interior of the eye-shaped regions are occupied by the border nodes of the ER network adopted in our simulations.

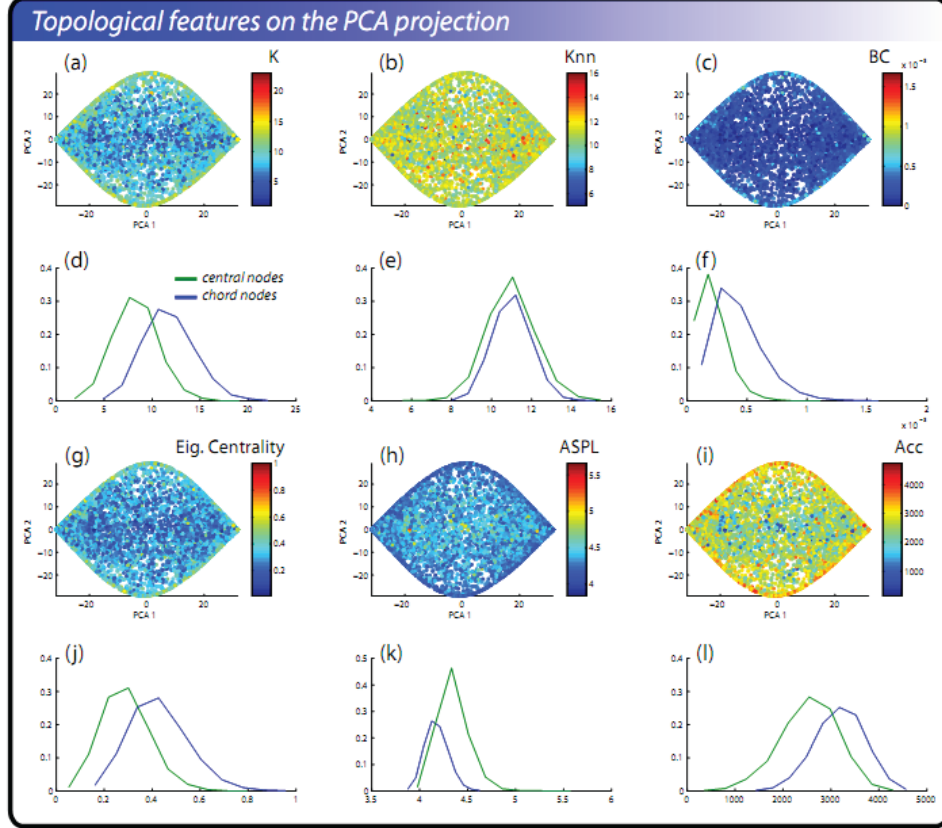


FIG. 7: 2D PCA projections of the time signals obtained for the SIS model colored in terms of the values of specific topological measurements (a-c, g-i). Histograms of the values of the topological measurements considering the time signals separation into chord and interior regions (d-f, j-l).

Acknowledgments

Luciano da F. Costa is grateful to FAPESP (05/00587- 5) and CNPq (301303/06-1 and 573583/2008-0) for the financial support. M. P. Viana was supported by a FAPESP grant (proc. 07/50882-9); J. L. B. Batista thanks CNPq (131309/2009-9) for sponsorship; and C. H. Comin is grateful to CAPES for his grant. The authors thank L. Baccalá for his remarks on clustered dynamics, and to G. Travieso and O. N. Oliveira for commenting on this work. The

authors also thank L. Antiqueira for help with box and for reading and commenting on the manuscript.

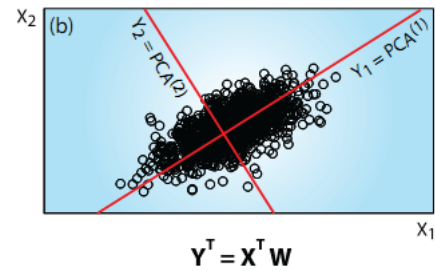
-
- [1] A. Barrat, M. Barthelemy, and A. Vespignani. *Dynamical Process on Complex Networks*. Cambridge University Press, Cambridge, UK, 2008.
 - [2] L. da F. Costa, O. N. Oliveira Jr., G. Travieso, F. A. Rodrigues, P. R. Villas Boas, L. Antiqueira, M. P. Viana, and L. E. C. Rocha. Analyzing and modeling real-world phenomena with complex networks: A survey of applications. *Advances in Physics*, 60(3):329–412, 2011.
 - [3] O. Sporns, D. R. Chialvo, M. Kaiser, and C. C. Hilgetag. Organization, development and function of complex brain networks. *Trends Cogn. Sci.*, 8(9):418–425, 2004.
 - [4] A. L. Barabási and Z. N. Oltvai. Network biology: Understanding the cell’s functional organization. *Nat. Rev. Genet.*, 5(2):101–U15, 2004.
 - [5] R. Pastor-Satorras and A. Vespignani. *Evolution and structure of the internet*. Cambridge University Press, 2004.
 - [6] C. Castellano, S. Fortunato, and V. Loreto. Statistical physics of social dynamics. *Rev. Mod. Phys.*, 81(2):591–646, 2009.
 - [7] M. E. J. Newman. The structure and function of complex networks. *SIAM Rev.*, 45:167, 2003.
 - [8] R. Albert and A. L. Barabási. Statistical mechanics of complex network. *Rev. Mod. Phys.*, 74:47–97, 2002.
 - [9] L. da F. Costa, F. A. Rodrigues, G. Travieso, and P. R. Villas Boas. Characterization of complex networks: A survey of measurements. *Adv. Phys.*, 56(1):167–242, 2007.
 - [10] S. Boccaletti, V. Latora, Y. Moreno, M. Chavez, and D.-U. Hwang. Complex networks: Structure and dynamics. *Phys. Rep.*, 424(4-5):175–308, 2006.
 - [11] S. N. Dorogovtsev, A. V. Goltsev, and J. F. F. Mendes. Critical phenomena in complex networks. *Rev. Mod. Phys.*, 80(4):1275–1335, 2008.
 - [12] I. T. Jolliffe. *Principal Component Analysis*. Springer, NY, 2002.
 - [13] M. Kaiser and C. C. Hilgetag. Nonoptimal component placement, but short processing paths, due to long-distance projections in neural systems. *PLoS Computational Biology*, 2(7):e95, 2006.
 - [14] C. Arndt. *Information Measures: Information and its Description in Science and Engineering*. Springer, 2004.
 - [15] X. Guardiola, A. Diaz-Guilera, M. Llas, and C. J. Perez. Synchronization, diversity, and topology of networks of integrate and fire oscillators. *Phys. Rev. E*, 62(4):5565–5570, 2000.
 - [16] A. Roxin, H. Riecke, and S. A. Solla. Self-sustained activity in a small-world network of excitable neurons. *Phys. Rev. Lett.*, 92(19):198101, 2004.
 - [17] R. Pastor-Satorras and A. Vespignani. Epidemic dynamics and endemic states in complex networks. *Phys. Rev. E*, 63(6):066117, 2001.
 - [18] R. Pastor-Satorras and A. Vespignani. Epidemic spreading in scale-free networks. *Phys. Rev. Lett.*, 86(14):3200–3203, 2001.
 - [19] H. Hong, M. Y. Choi, and B. J. Kim. Synchronization on small-world networks. *Phys. Rev. E*, 65(2):026139, 2002.
 - [20] Y. Moreno and A. F. Pacheco. Synchronization of kuramoto oscillators in scale-free networks. *Europhys. Lett.*, 68(4):603–609, 2004.
 - [21] A. Arenas, A. Daz-Guilera, J. Kurthsd, Y. Moreno, and C. Zhoug. Synchronization in complex networks. *Phys. Rep.*, 469(3):93–153, 2008.
 - [22] C. Koch. *Biophysics of computation: information processing in single neurons*. Oxford University Press, New York, 1999.
 - [23] A. N. Burkitt. A review of the integrate-and-fire neuron model: I. homogeneous synaptic input. *Biol. Cybern.*, 95(1):1–19, 2006.
 - [24] R. Pastor-Satorras and A. Vespignani. Epidemic dynamics and endemic states in complex networks. *Physical Review E*, 63:066117, 2001.
 - [25] B. Travenolo, M. P. Viana, and L. da F. Costa Border detection in complex networks. *New Journal of Physics*, 11(6):063019, 2009.

| | Integrate-and-Fire | | | Susceptible-Infected-Susceptible | | Kuramoto |
|-------------|--------------------|-------------|-------------|----------------------------------|-------------|-------------|
| Measurement | $PCA^{(1)}$ | $PCA^{(2)}$ | $PCA^{(3)}$ | $PCA^{(1)}$ | $PCA^{(2)}$ | $PCA^{(1)}$ |
| k | 2.52 | 2.67 | 2.24 | 1.28 | 1.51 | 0.15 |
| knn | 2.70 | 2.81 | 2.47 | 2.69 | 2.95 | 0.15 |
| BC | 2.50 | 2.62 | 2.22 | 1.62 | 1.95 | 0.15 |
| EC | 2.40 | 2.56 | 2.11 | 2.01 | 2.38 | 0.14 |
| ASPL | 2.43 | 2.60 | 2.14 | 2.00 | 2.37 | 0.13 |
| ACC | 2.43 | 2.60 | 2.15 | 2.12 | 2.48 | 0.13 |

TABLE I: The conditional entropies obtained for α considering the three dynamics in terms of some topological measurements: degree k , average neighbor degree knn , betweenness centrality BC , eigenvector centrality EC , average shortest path length $ASPL$ and accessibility ACC .

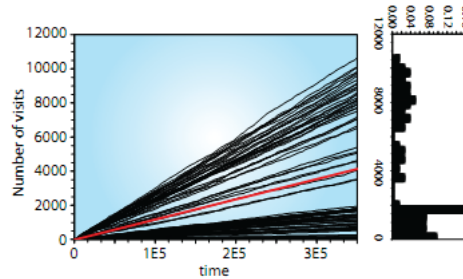
Principal component analysis

The multivariate method known as Principal Component Analysis (PCA) [12] aims at removing redundancies from a data set through the complete decorrelation of the original measurements. This is performed by rotating the coordinate axes so as to maximize the data dispersion along the first new axes or variables. Once the covariance of the original data is estimated, its eigenvalues are calculated and placed in decreasing order. These values correspond to the variance along the new axes. The eigenvectors respective to the largest eigenvalues are then used to build a linear transformation matrix \mathbf{W} that projects the data \mathbf{X} into the new coordinate system \mathbf{Y} through linear combinations of the original measurements, with weights given by the eigenvector components.



Structured dynamics

Diffusion in complex networks corresponds to one of the most Basic, and yet important, dynamics that can be investigated. The accompanying figure shows the number of visits at each node (black curves) along time in the diffusion in the giant component of a directed macaque cortical network of 85 nodes [13]. These curves tend to cluster into two well-defined groups of time signals. The straight line in red corresponds to the average values of the number of visits along time. The vertical histogram depicts the final densities. The obtained clusters provide the simplest example of structured dynamics.



Adopted dynamics

Integrate-and-Fire: Each neuron i integrates the signal of its incoming connections and fires whenever its internal state, ϕ_i , exceeds a threshold, τ , which can be described as:

$$\phi_i^{t+1} = \phi_i^t H(\tau - \phi_i^t) + \sum_j A_{ji} H(\phi_j^t - \tau)$$

where H is the Heaviside function.

Susceptible-Infected-Susceptible:

The model assumes that each node can be in two different states, Susceptible (S) or Infected (I). Each node in the state I can infect its neighbors with probability β . Infected nodes can also become susceptible with probability μ .

Kuramoto: It describes the collective behavior of N coupled oscillators with intrinsic frequencies ω_i ($i=1, \dots, N$). The set of equations governing their phases θ_i can be described as [7]:

$$\frac{d}{dt} \theta_i(t) = \omega_i + \frac{\lambda}{\langle k_i \rangle} \sum_j A_{ij} \sin(\theta_j - \theta_i)$$

where λ is the coupling strength.

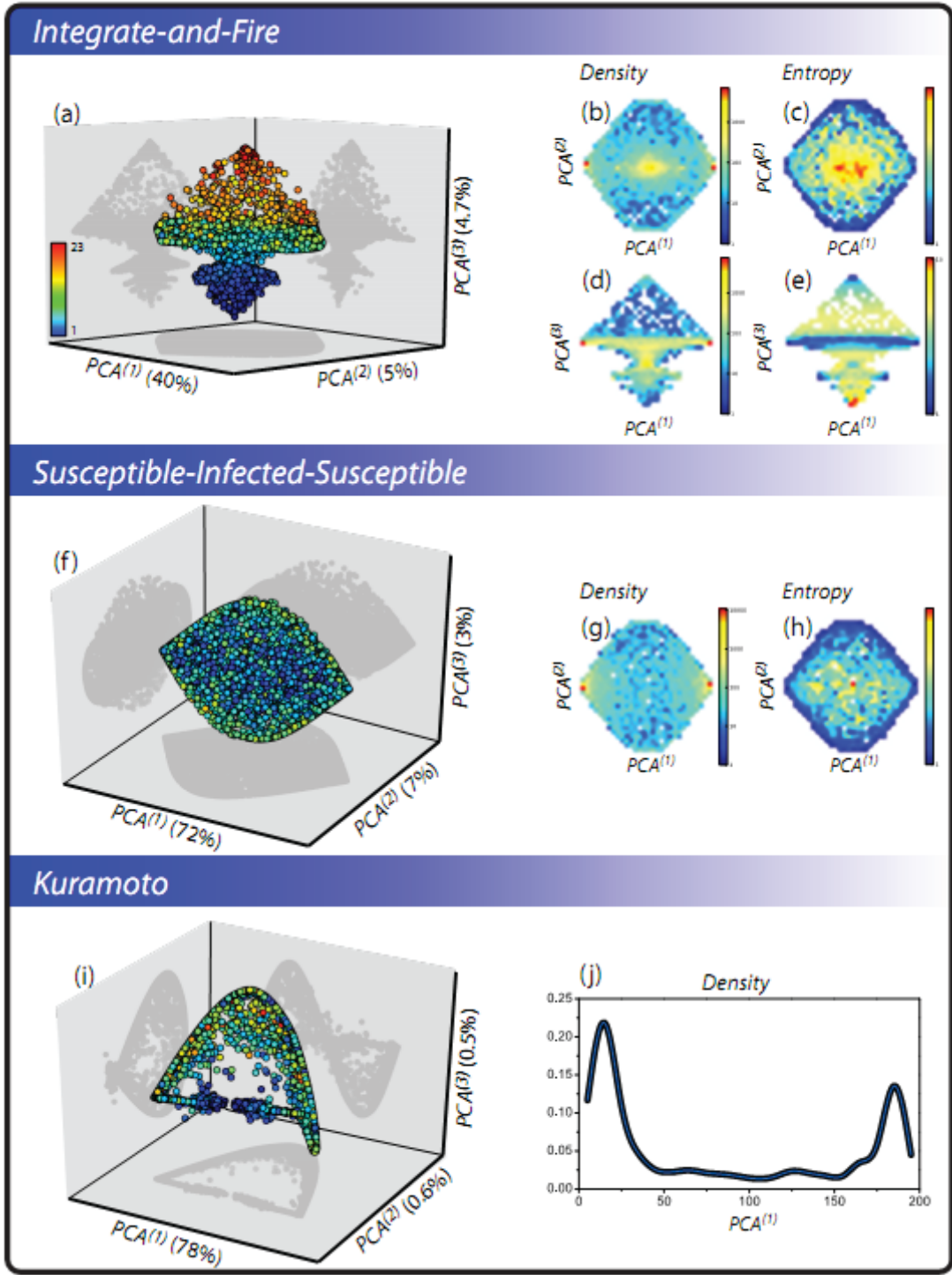


FIG. 8: The 3d PCA projections of the considered dynamics. (a)integrate-and-fire, (f)SIS, and (i)Kuramoto. The percentage of explained variance provided by each principal component variable are shown along each axis. The densities of the projections are shown in (b,d) for the integrate-and-fire, (g) for the SIS, and (j) for the Kuramoto. The respective signal entropies are depicted in (c,e) for the integrate-and-fire, (h) for the SIS. All these results were obtained for an ER network with 10000 nodes and average degree of 10. The integrate-and-fire realization considered initial conditions drawn uniformly within the range $[0, \tau + 1]$, with $\tau = 8$. The SIS dynamics assumed $\beta = 0.8$ and $\mu = 1$. The initial condition was such that 50% of the nodes were infected. The Kuramoto simulations were performed for $\kappa = 4$, with the natural frequencies drawn from a normal distribution with null mean and unit variance and the initial phases distributed uniformly between $[0, 2\pi]$. As shown in (b) and (d), the two extremities of the eye-shaped waist corresponds to approximately 40% of the nodes in the network. A third peak is found at the center of the ‘eye’, containing about 22% of the nodes. Likewise, in (g) the time signals concentrate at the two extremities of the ‘eye’, corresponding to about 55% of the nodes. The number of PCA axes considered were either enough to account for at least 75% of the variance or limited to 3.

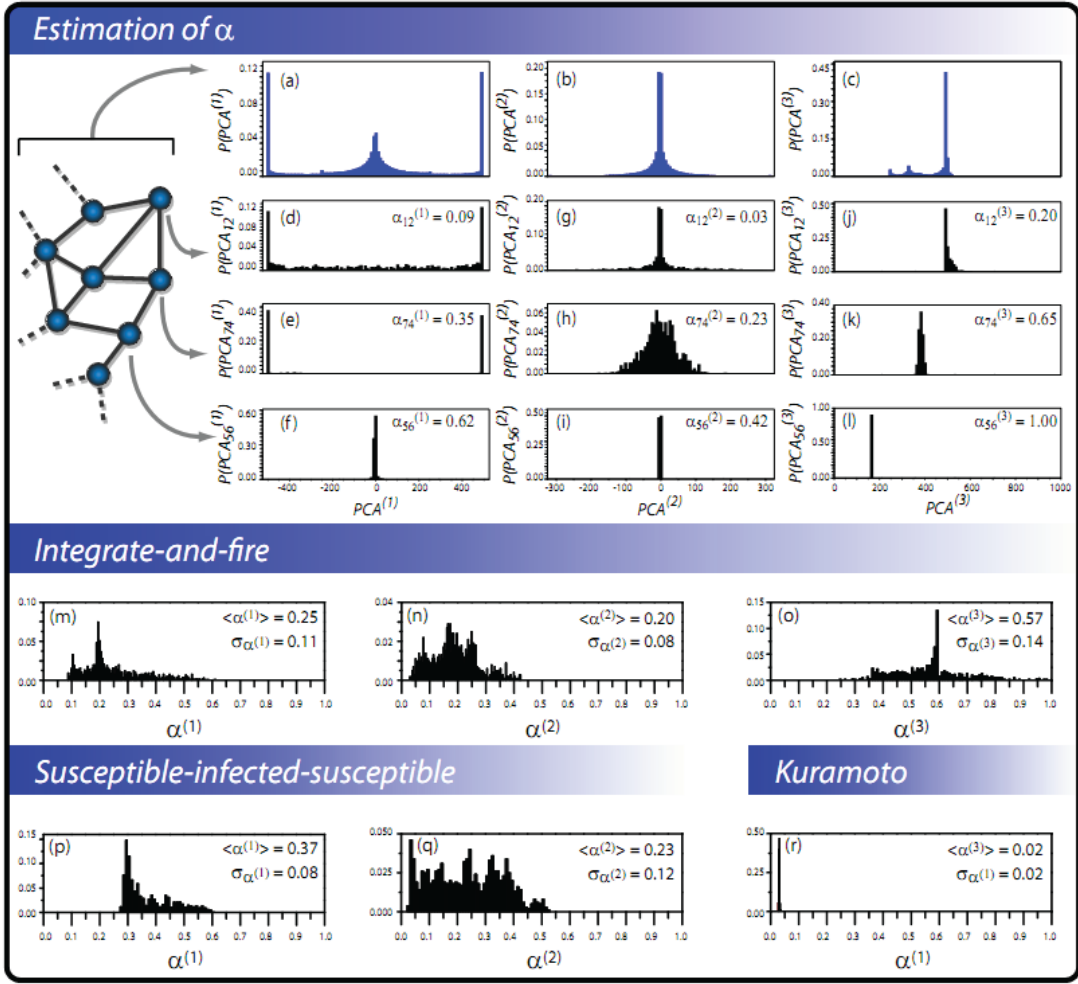


FIG. 9: *Estimation of the distribution of α .* The reference histograms of (a) $PCA^{(1)}$, (b) $PCA^{(2)}$ and (c) $PCA^{(3)}$ for 1000 realizations of the integrate-and-fire dynamics over the ER network with 1000 nodes and average degree 10. Examples of histograms (considering the same realizations) for specific nodes with respect to the (d-f) $PCA^{(1)}$, (g-i) $PCA^{(2)}$, and (j-i) $PCA^{(3)}$. The histograms of (m) $\alpha^{(1)}$, (n) $\alpha^{(2)}$ and (o) $\alpha^{(3)}$ for the integrate-and-fire dynamics; (p) $\alpha^{(1)}$, (q) $\alpha^{(2)}$ for the SIS dynamics; and (r) $\alpha^{(1)}$ for the Kuramoto dynamics. We used the same set of parameters as in Figure 8.

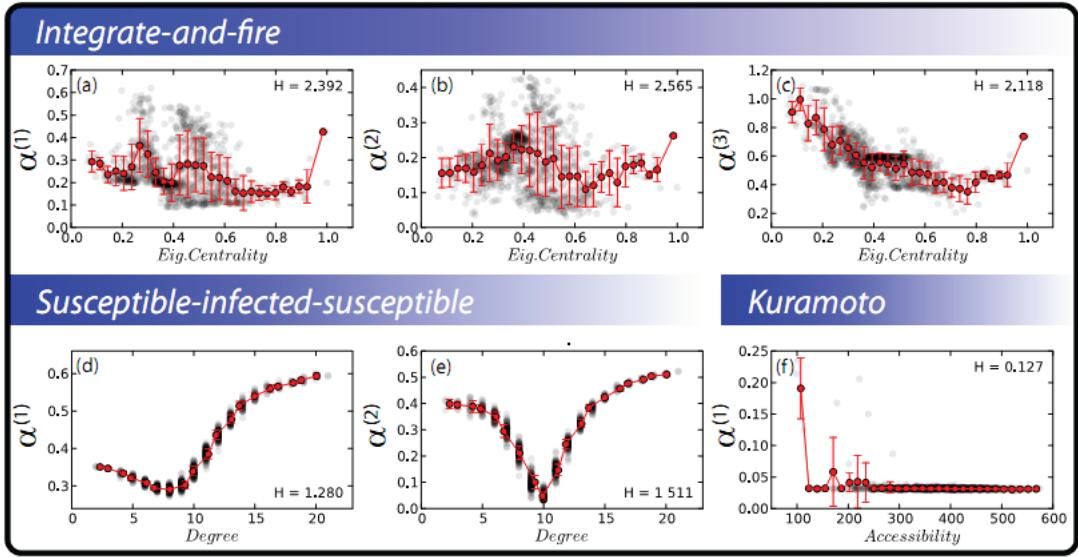


FIG. 10: Scatterplots between topological measurements and values of α : (a) $\alpha^{(1)} \times EC$, (b) $\alpha^{(2)} \times EC$, and (c) $\alpha^{(3)} \times EC$ for the integrate-and-fire dynamics; (d) $\alpha^{(1)} \times k$, and (e) $\alpha^{(2)} \times k$ for the SIS dynamics; and (f) $\alpha^{(1)} \times Acc$ for the Kuramoto dynamics. The red curve corresponds to the average of the α values, and bars indicate the standard deviation. Only the scatterplots obtained for the smallest conditional entropies in Table I are shown.